Carbohydrate Polymers 373 (2026) 124617

Contents lists available at ScienceDirect

Carbohydrate Polymers

journal homepage: www.elsevier.com/locate/carbpol

The impact of arabinose side chains on the swelling volume, water absorption, and thermal stability of peach gum polysaccharide

Jingyao Li [a,b], Mo Zhou [a,c,**], Jinfeng Bi [a,*], Aurore Richel [b]

[a] Key Laboratory of Agro-Products Processing and Storage, Ministry of Agriculture and Rural Affairs, Institute of Food Science and Technology, Chinese Academy of Agricultural Sciences, Beijing, 100193, China
[b] University of Liège, Gembloux Agro-Bio Tech, Passage des Déportés 2, 5030, Gembloux, Belgium
[c] Weifang Institute of Food Science and Processing Technology, Weifang, 261000, China

ARTICLE INFO

Keywords:
Peach gum
Polysaccharide
Debranching
Side chains
Swelling

ABSTRACT

Aiming to reveal the impact of side chains of peach gum polysaccharides (PGP) on its swelling ability, series PGP samples with different branching ratio (BR) (1.11–0.42) were prepared via α-L-arabinofuranosidase (10, 20, 40 μL) and trifluoroacetic acid (0.5, 1.0, 1.5 h) hydrolysis. Through characterization to the features of their branched structure, it showed that the debranched PGP samples retained the arabinogalactan body structure, presenting smaller MW, less extended molecular chains, and less cross-linking between PGP molecules. Methylation analysis indicated that enzymatic and short time acidic treatment mainly degraded the side chain of PGP, protecting the main chain from destruction. The swelling volume of PGP samples decreased from 0.43 cm^3 to 0.08 cm^3 with the decreasing BR. However, dynamic vapour sorption profiles revealed that the water absorption ability of PGP was not reduced with the degradation of side chains. This was explained by the changes of PGP network structure and improvement of thermal stability after debranching. This work provided novel knowledge for understanding "structure-property" relations of the arabinose side chains to the swelling properties of PGP.

1. Introduction

Peach gum (PG) is a natural plant gum secreted from peach tree (*Prunus persica* (L.) Batsch) after mechanical injuries or diseases to prevent further invasion of microorganisms (Bouaziz et al., 2016). It is one of the main by-products within the peach industrial chain. As the world's largest commercial peach producer, China produces about 10 billion tons of PG annually by estimation (Zhu et al., 2019). Accumulated studies have reported various health benefit functions of PG, such as hypoglycemic activity, antioxidant activity, and antibacterial activity (Chen et al., 2022; Yao et al., 2013). In China, PG has a long edible history and recently been approved as a new food material by the National Health Commission. However, the application of PG in food manufacturing is still limited currently, which is a huge waste of PG resource. This issue is mainly attributed to the "easily swelling-hardly dissolving" property of PG (Chen et al., 2022; Wei, Zhang, Zhang, et al., 2019).

The unique swelling property of PG is believed to be related to the structure of PG polysaccharide (PGP), which is the main component accounting for more than 95 % amount of PG. PGP belongs to the type II arabinogalactan family with a main chain consisting of β-D-(1 → 6)-galactose. Its side chains are mainly comprised of arabinose residues with various linkages. Currently identified side chains include α-L-Araf-(1→, α-L-Araf-(1 → 5)-α-L-Araf-(1→, →5)-α-L-Araf-(1→, and α-L-Araf-(1→3)-α-L-Araf-(1 → 3)-α-L-Araf- (1→, terminated by arabinose, xylose, rhamnose, glucose or glucuronic acid (Wei, Zhang, He, et al., 2019; Zhang et al., 2020). Our group has revealed the ultrasonic degradation of the galactose main chain of PGP could promote its solubility and alter its solution from non-Newtonian fluid to Newtonian fluid. In contrast, there is a lack of research revealing the role of side chains in PGP properties (Chen, Bi, et al., 2024; Chen, Zhou, et al., 2024).

Previous studies reported the impacts of the side chains on the properties of some polysaccharides such as pectin (Sousa et al., 2015), guar galactomannan (Mahammad et al., 2007), and mucilage

* Corresponding author at: Key Laboratory of Agro-Products Processing and Storage, Ministry of Agriculture and Rural Affairs, Institute of Food Science and Technology, Chinese Academy of Agricultural Sciences, Beijing, 100193, China.
** Corresponding author.
E-mail addresses: zhoumo@caas.cn (M. Zhou), bjfcaas@126.com (J. Bi).

https://doi.org/10.1016/j.carbpol.2025.124617
Received 8 June 2025; Received in revised form 8 October 2025; Accepted 27 October 2025
Available online 28 October 2025

arabinoxylan (Yu et al., 2017). Typical example is the pectin, which also contains arabinose side chains. Ngouémazong et al. (2012) reported that when 50 % of arabinose side chains were removed from carrot pectin, it showed poor ability to form gel with Ca^{2+} due to the reduction of polymer chain entanglements. Similar finding were observed in the case of watermelon rind pectin, where debranched samples showed lower apparent viscosity and weaker gelation network (Méndez et al., 2023). It could be summarized by these studies that the arabinose side chains possess strong water binding ability. Although swelling property is also related to water binding, it is distinct from gelling and rheological properties, since swelling is a kinetic process coupling mass transport and mechanical deformation, involving the change in macroscopic volume which depends on the interaction between the polymer network and the solvent (Bouklas & Huang, 2012). Currently, there are few studies focused on the effect of side chains on swelling properties, which remains knowledge gap on the role of PGP side chains in swelling property.

Based on previous studies, it is hypothesized that the swelling ability of PGP is closely related to the its branched structure. To validate this, a series of partial degraded PGP samples were prepared via enzymatic and acidic hydrolysis. The features of their branched structure were analyzed and compared with the original PGP sample. The swelling volume, water absorption, and thermal stability of debranched and original PGP sample were related to PGP network structure. This work would provide novel knowledge on "structure-property" relations of the arabinose side chains to the swelling properties of PGP.

2. Materials and methods

2.1. Materials

Crude PG was obtained at a peach farm (Suizhou, Hubei Province, China) from trunk and branch of trees, and then was ground into powder and passed through a 100 mesh sieve. The PG powder was stored in a desiccator at room temperature until use.

2.2. Preparation of original PGP sample

PG power (10 g) was dispersed into 95 °C water (1 L) with constant stirring for 3 h, and then the mixture was centrifuged (4900 r/min) at 20 °C for 30 min. The precipitate was extracted twice again according to the above steps. The supernatant was combined, vacuum concentrated, and dialyzed (3.5 kDa) against deionized water for 72 h, replacing the dialysis water every 8 h. Afterwards, the dialysis solution was freeze-dried to obtain the original PGP sample, which was designated as PGP-OR and stored in a desiccator at room temperature until use.

2.3. Preparation of partial debranched PGP samples

The PGP-OR sample was subjected to enzymatic and acidic hydrolysis for partial debranching, respectively. The enzymatic hydrolysis was performed via α-L-arabinofuranosidase (*Aspergillus niger*) (AFASE, 300 U/mL, Megazyme Co., UK) under its optimal conditions. Lyophilized PGP-OR (50 mg) was dispersed into 20 mL of 0.2 M phosphate buffer (pH 4.0) with constant stirring for 10 h to obtain 0.25 % (*w/v*) PGP-OR solution. Subsequently, the PGP-OR solution was incubated respectively with 10, 20, and 40 μL of AFASE (300 U/mL, Megazyme Co., UK) at 40 °C for 24 h. After incubation, the samples were immediately moved into 90 °C of water bath for 5 min to terminate the enzymatic reaction and then immediately cooled in ice bath. The acidic hydrolysis was performed via trifluoroacetic acid (TFA). Lyophilized PGP-OR (140 mg) was dispersed into 20 mL of 0.1 M TFA (Aladdin Co., USA) with constant stirring for 10 h to obtain 0.7 % (*w/v*) PGP-OR solution. The solution was kept in a water bath at 80 °C for 0.5 h, 1.0 h, and 1.5 h, respectively. Afterwards, the samples were immediately cooled in ice bath and neutralized by 0.2 M sodium hydroxide (NaOH) solution. The above enzymatic and acidic hydrolyzed solutions were dialyzed (3.5 kDa) against deionized water for 72 h, replacing the dialysis water every 8 h. Dialyzed samples were freeze-dried and stored in a desiccator at room temperature until further analyses. The samples treated by 10, 20, and 40 μL of AFASE hydrolysis were designated as PGP-EP10, PGP-EP20, and PGP-EP40, respectively. The samples treated by 0.5, 1.0, and 1.5 h of TFA hydrolysis were designated as PGP-AP0.5, PGP-AP1.0, and PGP-AP1.5, respectively.

2.4. Characterization of structural features of PGP samples

2.4.1. Monosaccharide composition

The monosaccharide composition of all PGP samples was determined following the method described by Chen et al. (2022) with some modifications. Lyophilized sample (10 mg) was dispersed into 2 mL of deionized water with constant stirring for 12 h. The sample solutions were fully hydrolyzed with 2 mL of 4 M TFA and then fully hydrolyzed at 110 °C for 2 h. After being cooled to room temperature and dried by nitrogen blowing, the sample was redissolved in deionized water and diluted to an appropriate concentration after filtration through 0.22 μm membrane. The diluted samples (10 μL) were analyzed by an ICS-3000 Ion Chromatography system (Dionex, Sunnyvale, CA, USA) on a Carbo Pac PA20 analytical column (Dionex) eluting with 250 mM NaOH at 35 °C with a flow rate of 0.5 mL/min. The monosaccharide standards, including arabinose (Ara), galactose (Gal), xylose (Xyl), rhamnose (Rha), glucose (Glc), and glucuronic acid (GlcA) (Sigma Chemical Co., USA) were used as external standards for identification and quantification.

2.4.2. Molecular weight (MW) distribution

The MW distribution parameters of all PGP samples were analyzed by a high performance size exclusion chromatography (HPSEC) system (Wyatt Technology, Santa Barbara, CA, USA) coupled with a multi-angle light scattering detector, a TSK gel column (TSK Gel G4000PWxl, 300 × 7.8 mm), a UV detector and a differential refractometer (RI). The analysis was followed the method described previously by Liu et al. (2023) with some modifications. Lyophilized sample (5 mg) was fully dissolved in 5 mL of 0.1 mol/L sodium chloride (NaCl) solution by constant stirring for 48 h. The sample solution was filtered through 0.45 μm filter membrane and then injected into the HPSEC system, eluted with 0.1 M NaCl solution at a flow rate of 0.5 mL/min for 30 min at 30 °C. Data were collected and analyzed by the online Astra software (Version 5.3.4, Wyatt Technology) with the refractive index increment (*dn/dc*) of 0.135 mL/g.

2.4.3. Intrinsic viscosity

Lyophilized PGP-OR, PGP-EPs, and PGP-APs samples were fully dissolved in deionized water and diluted to obtain a series of sample solutions at different concentrations, including 0.2, 0.4, 0.6, 0.8, and 1.0 mg/mL. The flow time of each solution passing through the Ubbelohde capillary viscometer (diameter = 0.52 mm) at 25 °C was recorded. The values of $[\eta]$ were calculated by the Huggins-Kramer equations as follows (Eqs. (1) and (2)):

$$\eta_{sp}/c = [\eta] + k[\eta]^2 c \quad (1)$$

$$ln(\eta_{rel})/c = [\eta] + (k - 0.5)[\eta]^2 c \quad (2)$$

where c is the concentration of sample, η_{sp} is the specific viscosity, η_{rel} is the relative viscosity.

2.4.4. Methylation analysis

The reduction of uronic acids of the polysaccharides were performed by using the method of methylation. Lyophilized PGP-OR, PGP-EP10, PGP-AP0.5, and PGP-AP1.0 samples (5 mg) were reduced with $NaBH_4$,

dialyzing and lyophilizing to acquire the reduzates. The reduzates were then methylated in DMSO/NaOH with CH_3I. After complete methylation, the permethylated products were hydrolyzed with 2 mol/L TFA at 121 °C for 1.5 h, reduced by $NaBD_4$ and acetylated with acetic anhydride for 2.5 h at 100 °C. The acetates were dissolved in chloroform and analyzed with GC–MS on an Agilent 6890A-5975C equipped with Agilent BPX70 chromatographic column (30 m × 0.25 mm × 0.25 μm) programmed from 140 °C and held for 2 min, increasing by 3 °C /min to 230 °C and hold for 3 min. Helium was used as the carrier gas with 1 mL/min. Mass spectra was interpreted to identify the compound that corresponded to each peak.

2.4.5. Fourier transform infrared (FTIR) scanning

The FTIR spectra of all PGP samples were measured by a Tensor 270 FTIR spectrometer (Bruker Co., USA) in the wavenumber range of 400 to 4000 cm^{-1} with the resolution of 4 cm^{-1}. Each sample was grounded with Kbr and pressed into 1 mm transparent flakes for analysis. Offline OPUS software (Version 5.0, Bruker Co.) was used for data collection and processing.

2.4.6. Atomic force microscopy (AFM) imaging

PGP-OR, PGP-EP40, and PGP-AP1.0 were selected to observe the apparent morphology by Bruker Dimension Icon AFM equipped with SCANASYST-Air probe. Lyophilized sample was dispersed into deionized water with ultrasonic dispersion for 10 min and further diluted to appropriate concentration. The filtrate (10 μL) was dripped onto the center of a flat mica surface and allowed to dry at room temperature before AFM imaging.

2.5. Measurement of swelling volume

Lyophilized PGP-OR, PGP-EPs, and PGP-APs samples were immersed in distilled water at a ratio of 1:100 (*w/w*) for 120 min to reach equilibrium swelling. Afterwards, the mixtures were centrifuged (12,000 rpm) at 25 °C for 15 min to separate the supernatant and hydrogel. The mass of the hydrogel was recorded. The density of hydrogel was calculated by sucking a defined mass of hydrogel into a defined volume of syringe. The swelling volume (v) was calculated by the mass (m) over density (ρ).

2.6. Profiling of dynamic vapour sorption (DVS) curve

The water absorption of lyophilized PGP samples were determined by a DVS analyzer (Surface Measurement Systems Ltd., London, UK) equipped with a Cahn microbalance. The experiments were carried out at 25 °C with relative humidity (RH) from 0 % to 90 %. Each sample (10 mg) was dehydrated in the DVS chamber at 0 % RH until reaching the equilibrium mass and then subjected to hydration at 90 % RH. The mass equilibrium at each humidity was determined using a dm/dt (mass variation over time variation) of 0.002 %/min. The sample mass (m) was monitored with hydration time (t).

2.7. Scanning electron microscopy (SEM) imaging analysis

Scanning electron microscopy (SEM) (SU8010, Hitachi Co., Tokyo, Japan) observation was performed on the PGP-OR, PGP-EP10, PGP-AP0.5, and PGP-AP1.0 samples at their water adsorption equilibrium state. Before observation, the samples underwent a dynamic vapour sorption to reach adsorption equilibrium, and then freeze-dried. The cross-section of samples was cut with a razor blade at the same place (center of samples), and then fixed to an aluminum stub using double sided sticky tape, followed by the gold coating for 30 s using an ion sputtering apparatus (MCI000, Hitachi Co., Tokyo, Japan). The magnification was of 300 ×. The images were captured at 5 kV accelerated voltage and 8–11.5 mm working distance.

Table 1
Monosaccharides composition and branching ratio (BR) of original and debranched peach gum polysaccharides.

	PGP-OR	PGP-EP10	PGP-EP20	PGP-EP40	PGP-AP0.5	PGP-AP1.0	PGP-AP1.5
Ara (mg/g)	230.63 ± 13.54 ^{a} (43.66 %)	186.06 ± 12.26 ^{b} (42.62 %)	185.51 ± 13.70 ^{b} (42.31 %)	159.53 ± 6.09 ^{c} (40.69 %)	140.40 ± 8.09 ^{cd} (35.50 %)	118.87 ± 2.57 ^{de} (26.73 %)	103.58 ± 10.36 ^{e} (24.65 %)
Gal (mg/g)	209.09 ± 15.45 ^{b} (39.56 %)	179.82 ± 6.22 ^{cd} (41.22 %)	177.79 ± 10.09 ^{cd} (40.40 %)	162.33 ± 4.42 ^{d} (41.45 %)	190.43 ± 12.66 ^{bc} (48.13 %)	247.24 ± 1.83 ^{a} (55.59 %)	249.66 ± 5.76 ^{a} (59.39 %)
Xyl (mg/g)	61.37 ± 1.93 ^{a} (11.65 %)	46.24 ± 2.56 ^{ab} (10.59 %)	49.17 ± 14.00 ^{ab} (11.07 %)	43.95 ± 9.49 ^{b} (11.18 %)	40.32 ± 2.67 ^{b} (10.19 %)	45.29 ± 2.30 ^{ab} (10.18 %)	39.05 ± 4.36 ^{b} (9.29 %)
Rha (mg/g)	2.81 ± 0.09 ^{a} (0.53 %)	2.05 ± 0.29 ^{ab} (0.47 %)	2.91 ± 0.64 ^{a} (0.64 %)	1.49 ± 0.53 ^{b} (0.38 %)	1.49 ± 0.00 ^{b} (0.38 %)	2.40 ± 0.33 ^{ab} (0.54 %)	1.89 ± 0.20 ^{b} (0.45 %)
Glc (mg/g)	2.93 ± 1.74 ^{abc} (0.57 %)	1.79 ± 0.37 ^{c} (0.41 %)	2.51 ± 1.79 ^{bc} (0.60 %)	4.16 ± 0.20 ^{abc} (1.06 %)	4.91 ± 0.36 ^{ab} (1.24 %)	5.35 ± 0.27 ^{a} (1.20 %)	2.44 ± 0.10 ^{c} (0.58 %)
GlcA (mg/g)	21.42 ± 5.35 ^{ab} (4.03 %)	20.45 ± 0.09 ^{ab} (4.69 %)	21.91 ± 2.48 ^{ab} (4.99 %)	20.56 ± 1.83 ^{ab} (5.24 %)	18.02 ± 1.23 ^{b} (4.56 %)	25.61 ± 1.24 ^{a} (5.76 %)	23.68 ± 1.89 ^{ab} (5.64 %)
BR (Ara/Gal)	1.11 ± 0.02 ^{a}	1.04 ± 0.04 ^{ab}	1.03 ± 0.08 ^{ab}	0.98 ± 0.07 ^{b}	0.74 ± 0.01 ^{c}	0.48 ± 0.01 ^{d}	0.42 ± 0.01 ^{d}

PGP-OR: original peach gum polysaccharide extracted by hot water.
PGP-EP10, PGP-EP20, and PGP-EP40: the samples hydrolyzed from PGP-OR by 10, 20 and 40 μL of α-L-arabinofuranosidase treatment, respectively.
PGP-AP0.5, PGP-AP1.0, and PGP-AP1.5: the samples hydrolyzed from PGP-OR by 0.5, 1.0 and 1.5 h of trifluoroacetic acid treatment, respectively.
Ara: arabinose; Gal: galactose; Xyl: xylose; Rha: Rhamnose; Glc: Glucose; GlcA: Glucuronic acid.
Results are presented as mean values (± standard error) of three replicates ($n = 3$).
Values in the same row with different letters are significantly different at $p < 0.05$.

Table 2
The molecular weight and conformational parameters of original and debranched peach gum polysaccharides.

Parameters	PGP-OR	PGP-EP10	PGP-EP20	PGP-EP40	PGP-AP0.5	PGP-AP1.0	PGP-AP1.5
M_n ($\times 10^6$ g/mol)	5.72 ± 0.03 ^{b}	5.33 ± 0.15 ^{c}	5.05 ± 0.05 ^{d}	5.85 ± 0.08 ^{b}	6.71 ± 0.08 ^{a}	4.51 ± 0.04 ^{e}	3.95 ± 0.03 ^{f}
M_w ($\times 10^6$ g/mol)	13.26 ± 0.03 ^{a}	6.90 ± 0.22 ^{e}	6.27 ± 0.06 ^{g}	7.85 ± 0.01 ^{c}	11.43 ± 0.06 ^{b}	7.59 ± 0.13 ^{d}	6.57 ± 0.07 ^{f}
M_w/M_n	2.32 ± 0.01 ^{a}	1.30 ± 0.01 ^{e}	1.24 ± 0.01 ^{f}	1.34 ± 0.02 ^{d}	1.70 ± 0.01 ^{b}	1.68 ± 0.01^{bc}	1.67 ± 0.03 ^{c}
[η] (dL/g)	15.43 ± 0.14 ^{b}	6.58 ± 0.12 ^{de}	6.25 ± 0.06 ^{e}	6.91 ± 0.09 ^{d}	15.32 ± 0.02 ^{b}	16.06 ± 0.04 ^{a}	14.32 ± 0.51 ^{c}
R_g (nm)	212.85 ± 1.63 ^{a}	107.20 ± 3.96 ^{e}	97.05 ± 0.78 ^{f}	121.80 ± 1.56 ^{d}	206.70 ± 0.42 ^{a}	160.50 ± 5.23 ^{b}	147.40 ± 4.81 ^{c}
R_h (nm)	148.24 ± 0.44 ^{a}	89.67 ± 0.55 ^{f}	85.34 ± 0.30 ^{g}	95.15 ± 0.40 ^{e}	140.48 ± 0.05 ^{b}	124.60 ± 0.11 ^{c}	114.29 ± 1.37 ^{d}
ρ (R_g/R_h)	1.44 ± 0.01 ^{b}	1.20 ± 0.01 ^{d}	1.14 ± 0.01 ^{e}	1.28 ± 0.01 ^{c}	1.47 ± 0.01 ^{a}	1.29 ± 0.01 ^{c}	1.26 ± 0.02 ^{c}

PGP-OR: original peach gum polysaccharide extracted by hot water.
PGP-EP10, PGP-EP20, and PGP-EP40: the samples hydrolyzed from PGP-OR by 10, 20 and 40 μL of α-L-arabinofuranosidase treatment, respectively.
PGP-AP0.5, PGP-AP1.0, and PGP-AP1.5: the samples hydrolyzed from PGP-OR by 0.5, 1.0 and 1.5 h of trifluoroacetic acid treatment, respectively.
Results are presented as mean values (± standard error) of three replicates ($n = 3$).
Values in the same row with different letters are significantly different at $p < 0.05$.

2.8. Measurement of differential scanning calorimetry (DSC)

The PGP-OR, PGP-EP10, PGP-AP0.5, and PGP-AP1.0 were selected to determine the T_g and enthalpy change (ΔH) using a DSC instrument (Model Q200, TA Instruments, New Castle, DE, USA). Lyophilized sample (approximately 3 mg) was placed in an aluminum DSC pan and hermetically sealed. The samples were heated from 30 °C to 160 °C at a heating rate of 10 °C/min. The DSC heat flow curves were analyzed by specialized software (Universal Analysis, TA, US). The T_g was determined from the midpoint of the endothermic shift, and ΔH was calculated from the peak area between the onset and end temperature.

2.9. Statistical analysis

All data were yielded from at least three independent experiments. One-way analysis of variance (ANOVA, Duncan test) was performed using SPSS Statistics 20 (Chicago, IL, USA). Significant differences ($p < 0.05$) among multiple groups were identified using Duncan test.

3. Results and discussion

3.1. Monosaccharide composition of PGP samples

In order to evaluate the debranched effectiveness of enzymatic and acidic hydrolysis, the contents of individual monosaccharides of all PGP samples were determined and the results are shown in Table 1. The amounts of Ara and Gal of PGP-OR were close, which were 230.63 ± 13.54 (43.66 %) and 209.09 ± 15.45 (39.56 %) mg/g, respectively. They accounted for the majority of total monosaccharide content, indicating the arabinogalactans structure of PGP. Since the main chain and side chains of PGP are mainly composed of Gal and Ara respectively, the content ratio of Ara over Gal could be used to estimate the branching ratio (BR) of PGP. The BR value of PGP-OR was 1.1, indicating a highly branched structure. Besides Ara residues, previous studies reported the side chains of PGP might also contain Xly and GlcA (Wei, Zhang, He, et al., 2019). Therefore, the certain amount of Xyl (61.37 ± 1.93 mg/g) and GlcA (21.42 ± 5.35 mg/g) further suggested the branched structure of PGP-OR was complicated. Meanwhile, small amount of Rha (2.81 ± 0.09 mg/g) and Glc (2.93 ± 1.74 mg/g) were also detected in PGP-OR.

After AFASE treatment, it was as expected that the Ara contents of PGP-EP10, PGP-EP20, and PGP-EP40 all decreased to some extent, with the values of 186.06 ± 12.26 (42.62 %), 185.51 ± 13.70 (42.31 %), and 159.53 ± 6.09 (40.69 %) mg/g, respectively. It suggested that AFASE successful hydrolyzed part of the Ara chain of PGP-OR. When the dosage of AFASE to 50 mg of PGP was 12 units of enzyme activity, the Ara content decreased by 71.10 mg/g. Meanwhile, the Gal content decreased synchronously with the Ara after AFASE hydrolysis, which suggested that there might be an Ara-Gal linkage in the molecular chain of PGP-OR. Since Ara is primarily localized in the side chains of the PGP-OR, it was a high probability that there was portion of Gal residues in the side chains of PGP-OR, which was linked with Ara residue with α-1,2-, α-1,3- or α-1,5 linkage that could be hydrolyzed by AFASE (Zhang et al., 2020). Although the content of Ara and Gal both reduced, the BR values of all PGP-EPs still decreased to about 1.0, which indicated that the proportion of branched chains reached to equal level with the main chains. On the other hand, the reduction of BR values after AFASE treatment were only about 10 % compared to PGP-OR and no significant differences existed among the three PGP-EP samples. This indicated that enzymatic debranching by AFASE was limited and inefficient, resulted in a high percentage of Ara still being retained.

Mild acid (0.1 M, TFA) treatment has been successfully used to partially hydrolyze the Ara side chains of arabinogalactan (Peng et al., 2016; Simas et al., 2008). In this study, the results showed that TFA treatment was more effective on the degradation of Ara chains than AFASE treatment, since the Ara contents of PGP-AP0.5, PGP-AP1.0, and PGP-AP1.5 were 140.40 ± 8.09 (35.50 %), 118.87 ± 2.57 (26.73 %), 103.58 ± 10.36 (24.65 %) mg/g, respectively, which were significantly lower than that of PGP-EP samples. Furthermore, the degraded level of Ara chains was increased with TFA treating time. Unlike the synchronized decreases of Gal and Ara after AFASE hydrolysis, among three PGP-AP samples, only PGP-AP0.5 appeared a decreased Gal content, which was 190.43 ± 12.66 (48.13 %) mg/g. The other two showed an increased Gal contents, which were 247.24 ± 1.83 (55.59 %) and 249.66 ± 5.76 (59.39 %) mg/g for PGP-AP1.0 and PGP-AP1.5, respectively. This phenomenon generally occurred in excessive hydrolysis of a sample resulting in an increase content of individual monosaccharide per unit mass of the sample. For instance, Simas et al. (2008) previously reported that the Gal content increased after acidic hydrolysis of PGP. The BR values of PGP-AP samples were 0.74 ± 0.01, 0.48 ± 0.01, and 0.42 ± 0.01 respectively, which were significantly lower than those of PGP-EP samples. Therefore, a series of debranched PGP samples with gradient reduced BR were successfully prepared through AFASE and TFA hydrolysis. However, the variation patterns of Ara and Gal were different between PGP-EP and PGP-AP samples. It might indicate the different chain broken mechanisms of PGP side chains under AFASE and TFA treatment, which need further analysis.

3.2. MW parameters of PGP samples

The MW parameters of all PGP samples were analyzed to further investigate the impacts of debranching on the structure of PGP. As listed in Table 2, the M_w of PGP-OR was 13.30 ± 0.01 × 10^6 g/mol, which was close to the previous reported data of the hot water extracted PGP (Chen et al., 2022), indicating a super large molecule size. After enzymatic debranching, it was as expected that the M_w decreased, with the values of 6.90 ± 0.22 × 10^6, 6.27 ± 0.06 × 10^6, 7.85 ± 0.01 × 10^6 g/mol for PGP-EP10, PGP-EP20, and PGP-EP40 respectively. In the case of acidic debranching, the M_w decreased gradually with treating time, with the values of 11.43 ± 0.01 × 10^6, 7.59 ± 0.13 × 10^6, 6.57 ± 0.07 × 10^6 g/mol for PGP-AP0.5, PGP-AP1.0, and PGP-AP1.5 respectively. Although

the BR values of PGP-APs were significantly lower than those of PGP-EP samples, their M_w values were at the same level with PGP-EPs, even obviously higher in the case of PGP-AP0.5. This might further suggest the different impacts of AFASE and TFA debranching on PGP structure, which could be better understood through the polydispersity index (M_w/M_n). The polydispersity index of PGP-OR (2.32 ± 0.01) was the highest among all samples, which indicated that PGP-OR was a highly heterogeneous polysaccharide. Both AFASE and TFA debranching could decrease the polydispersity index, with the values of 1.30 ± 0.01, 1.24 ± 0.01, and 1.34 ± 0.02 for PGP-EPs and 1.70 ± 0.01, 1.68 ± 0.01, and 1.67 ± 0.03 for PGP-APs, respectively. The significantly lower values of PGP-EPs compared to PGP-APs indicated the molecular size of the hydrolyzed products generated by AFASE debranching was more uniform than that generated by TFA debranching. This could be attributed to the specific chain-breaking site of AFASE hydrolysis, which was targeted at α-1,2-, α-1,3-, and α-1,5-linked L-arabinofuranose residues. Therefore, most of the cut products were Ara residues that had been removed by dialysis before analysis. In comparison, the breaking sites of PGP molecular chains were random by TFA hydrolysis. It meant that the cut products might contain large fragments consisting of Gal or other residues that could not be removed by dialysis before analysis, which contributed an increasing of heterogenization that reflected in the M_w/M_n.

3.3. Conformational parameters of PGP samples

The values of intrinsic viscosity ([η]), *Z*-average radius of gyration (R_g) and hydrodynamic radius (R_h) could help to understand the structural alterations of PGP-OR after AFASE and TFA hydrolysis from the aspect of molecular conformation, which are shown in Table 2. The [η] values of a given structured polysaccharide represent the hydrodynamic volume occupied by the macromolecule itself in a given solvent, which is positively correlated with MW according to the Mark-Houwink equation ($[\eta] = KM^{\alpha}$). The [η] of PGP-OR was 15.43 ± 0.14 dL/g, which decreased to 6.25 ± 0.06–6.91 ± 0.09 dL/g after AFASE hydrolysis paralleling with decreased M_w values. It suggested that AFASE debranching did not destroy the primary structure of PGP and the molecules of PGP-EPs were less extended than PGP with the decreasing BR. However, the [η] values were not decreased after TFA hydrolysis, which was not positively correlated with the variations of their M_w values. Although the M_w of PGP-APs decreased, their [η] were still retained at a high level, with the values of 15.32, 16.06, and 14.32 dL/g, respectively. The [η] value generated by a single molecule with the extreme dilution which reflects the intermolecular interaction (He et al., 2023). The relative higher [η] value of PGP-APs than PGP-EPs indicated a stronger intermolecular motion resistance between PGP-APs and water molecules, which might be due to more functional groups exposed after acidic debranching.

R_g and R_h are important conformational parameters to characterize the actual space occupied by the polymer chains. R_g was obtained directly by HPSEC analysis and R_h was estimated by the Einsteine-Simha relation ($R_h = (3M_w[\eta]/10\pi N_A)^{1/3}$) (Fishman et al., 2015). The PGP-OR possessed the highest R_g and R_h values among all samples, which could be attributed to its highest M_w and [η]. After AFASE and TFA hydrolysis, the R_g and R_h values decreased, owing to partial degradation of molecular chain reducing the molecular size of PGP-EPs and PGP-APs. Meanwhile, it should be noted that the R_g and R_h values of PGP-APs were higher than those of PGP-EPs, which was consistent with the variation pattern of [η] values. It was probably due to the fact that the random degradation of side chains by TFA remained some long chains, therefore the actual occupied space of the molecule was not reduced a lot.

The ratio of R_h and R_g (ρ) is used to characterize the shape of a polymer in solution, including long chains, semi-flexible chains, and compact spheres. Their corresponding ρ values were 2, 1.5–1.8, and 0.775 in aqueous solution (Yang & Zhang, 2009). The ρ value of PGP-OR was 1.44, which was close to 1.5, indicating that its conformation tended to be semi-flexible chains. After AFASE hydrolysis, the ρ values decreased to 1.14–1.28, which indicated that the conformation of PGP-EPs might be at the state between semi-flexible chains and compact spheres. This result could be attributed to the decreased MW and BR of PGP-EPs, resulting in a reduced extended degree of molecular chains. After TFA hydrolysis, the ρ value of PGP-AP0.5 was 1.47, which was close to PGP-OR, indicating an approximate semi-flexible chains conformation. The ρ values of PGP-AP1.0 and PGP-AP1.5 were 1.29 and 1.26 respectively, which were close to those of PGP-EPs, indicating an intermediate state of semi-flexible chains and compact spheres.

Table 3
Linkage patterns and corresponding percentage of sugar residues in PGP-OR, PGP-EP10, PGP-AP0.5, and PGP-AP1.0 from methylation and GC–MS analysis.

RT (min)	PMAA	Linkage type	Molar ratio (%)			
			PGP-OR	PGP-EP10	PGP-AP0.5	PGP-AP1.0
Arabinose						
4.90	2,3,5-Me_3-Ara	Ara*f*-(1→	23.98	26	28.34	17.55
5.93	2,3,4-Me_3-Ara	Ara*p*-(1→	5.18	1.27	1.36	1.45
7.74	2,5-Me_2-Ara	→3)-Ara*f*-(1→	2.82	–	6.09	3.26
9.02	2,3-Me_2-Ara	→5)-Ara*f*-(1→	7.07	12.51	12.86	12.52
Galactose						
8.31	2,3,4,6-Me_4-Gal	Gal*p*-(1→	–	–	–	3.05
13.25	2,3,4-Me_3-Gal	→6)-Gal*p*-(1→	–	–	4.17	4.06
10.91	2,4,6-Me_3-Gal	→3)-Gal*p*-(1→	8.23	10.06	5.49	9.17
11.86	2,3,6-Me_3-Gal	→4)-Gal*p*-(1→	–	–	–	10.48
13.71	2,6-Me_2-Gal	→3,4)-Gal*p*-(1→	1.83	3.48	3.21	2.42
16.79	2,4-Me_2-Gal	→3,6)-Gal*p*-(1→	17.65	14.69	12.22	13.49
18.20	2-Me-Gal	→3,4,6)-Gal*p*-(1→	7.59	5.44	8.36	3.43
Other sugars						
6.08	2,3,4-Me_3-Xyl	Xyl*p*-(1→	7.53	7.54	5.56	4.18
12.49	3-Me-Xyl	→2,4)-Xyl*p*-(1→	1.16	1.21	1.89	1.31
7.42	2,3,4,6-Me_4-Glc	Glc*p*-UA-(1→	4.83	5.06	3.97	4.40
12.23	2,3,6-Me_3-Glc	→4)-Glc*p*-(1→	4.79	4.82	2.31	3.91
13.01	4,6-Me_2-Man	→2,3)-Man*p*-(1→	7.34	7.92	4.17	5.32

PGP-OR: original peach gum polysaccharide extracted by hot water.
PGP-EP10: the sample hydrolyzed from PGP-OR by 10 μL of α-L-arabinofuranosidase treatment.
PGP-AP0.5: the sample hydrolyzed from PGP-OR by 0.5 h of trifluoroacetic acid treatment.
PGP-AP1.0: the sample hydrolyzed from PGP-OR by 1.0 h of trifluoroacetic acid treatment;
RT: Retention time; –: no data.
The percentages of each sugar residue were calculated according to the peak areas from the total ion chromatograph of PMAA.

3.4. Methylation and GC–MS analysis

In order to further analyze the debranching effect after enzymatic and acid hydrolysis, PGP-OR, PGP-EP10, PGP-AP0.5, and PGP-AP1.0

were subjected to methylation and GC–MS analysis (Table 3). In the case of PGP-OR, the Ara related residues including Ara*f*-(1 → (23.98 %), Ara*p*-(1 → (5.18 %), →3)-Ara*f*-(1 → (2.82 %), and →5)-Ara*f*-(1 → (7.07 %) totally accounted for 39.05 %, meanwhile the Gal related residues including →3)-Gal*p*-(1 → (8.23 %), →3,4)-Gal*p*-(1 → (1.83 %), →3,6)-Gal*p*-(1 → (17.65 %), and →3,4,6)-Gal*p*-(1 → (7.59 %) totally accounted for 35.30 %. The other residues included Xyl*p*-(1 → (7.53 %), →2,4)-Xyl*p*-(1 → (1.16 %), Glc*p*-UA-(1 → (4.83 %), →4)-Glc*p*-(1 → (4.79 %), and →2,3)-Man*p*-(1 → (7.34 %). Coupled with the fine structure of PGP depicted by previous studies, the positions of the above sugar residues within the molecular chain could be deduced (Simas et al., 2008; Wei, Zhang, He, et al., 2019; Zeng et al., 2022). The →3,6)-Gal*p*-(1→ and →3,4,6)-Gal*p*-(1→ composed the main chain, while →3)-Ara*f*-(1→, →5)-Ara*f*-(1→, →3)-Gal*p*-(1→, →3,4)-Gal*p*-(1→, →2,4)-Xyl*p*-(1→, →4)-Glc*p*-(1→, and →2,3)-Man*p*-(1→ were located on the side chains. Particularly, the residues of →3)-Ara*f*-(1→, →5)-Ara*f*-(1→, and Ara-(1→ were directly connected to the main chain. The residues of Ara*f*-(1→, Ara*p*-(1→, Xyl*p*-(1→, and Glc*p*-UA-(1→ were at the end of molecular chains.

After enzymatic debranching, the →3)-Ara*f*-(1→ residue was not detected in PGP-EP10, since the AFASE predominantly acted on α-1,3-linked arabinofuranose. As the 3)-Ara*f*-(1→ unit was located at the junction of the main chain, its removal resulted in a decrease in the substitution degree of the main chain. Correspondingly, the →3,6)-Gal*p*-(1→ and →3,4,6)-Gal*p*-(1→ residues in the main chain decreased to 14.69 % and 5.44 %, respectively. The terminal Ara*p* also decreased to 1.27 %. These results indicated that enzymatic debranching was more targeted, mainly degrading 1, 3-Ara and terminal Ara. Their degradation led to a relative increase in the molar ratios of other residues, including Ara*f*-(1 → (26 %), →5)-Ara*f*-(1 → (12.51 %), →3)-Gal*p*-(1 → (10.06 %), and →3,4)-Gal*p*-(1 → (3.48 %). The molar ratio of other sugars remained stable.

After acidic debranching, it could be noted that →6)-Gal*p*-(1→ residue was detected in both PGP-AP0.5 and PGP-AP1.0 samples, with the molar ratio of 4.17 % and 4.06 %, which were not detected in PGP-OR and PGP-EP10 samples. This residue was directly hydrolyzed from →3,6)-Gal*p*-(1→ residue of the main chain, whose molar ratio correspondingly decreased to 12.22 % and 13.49 % in PGP-AP0.5 and PGP-AP1.0, respectively. The residue released from the O-3 position of →3,6)-Gal*p*-(1→ was →3)-Ara*f*-(1→, which was increased after acidic treatment. In addition, acidic treatment also decreased the molar ratio of side chain units and terminal units, including →3)-Gal*p*-(1→, Xyl*p*-(1→, Glc*p*-UA-(1→, →4)-Glc*p*-(1→, and →2,3)-Man*p*-(1→. Particularly, Gal*p*-(1→ and →4)-Gal*p*-(1→ were only detected in PGP-AP1.0. Together with the obviously decreased molar ratio of →3,4,6)-Gal*p*-(1 → (3.43 %), it could be deduced that the backbone of PGP-AP1.0 occurred cleavage, which was evidenced by the removal at the O-6 position linkage. The degradation of terminal residues might exposed Gal residues which were located in the side chain. Therefore, Gal*p*-(1→ was detected in PGP-AP1.0.

In summary, PGP-EP10 and PGP-AP0.5 retained the Gal main chain but their side chains were removed to different degrees, while the main chain of PGP-AP1.0 was partially disrupted. Together with the preceding discussion on the results of monosaccharide composition and MW parameters, it revealed the different pattern between enzymatic and acidic debranching.

In order to more actually quantify the variation of side chains after debranching, beside the BR values which have been presented in Table 1, we introduced the degree of branching (DB) value which was calculated by the following equation:

$$DB = (NT + NB)/(NT + NB + NL) \quad (3)$$

where NT, NB, and NL represent the number of terminal, branched and linear residues, respectively.

The DB values of PGP-OR, PGP-EP10, PGP-AP0.5, and PGP-AP1.0 gradually decreased, with 77.09 %, 72.61 %, 69.08 %, and 56.6 %, respectively. This was consistent with the trend in BR values, further suggesting the different debranching effectiveness of enzymatic and acidic hydrolysis.

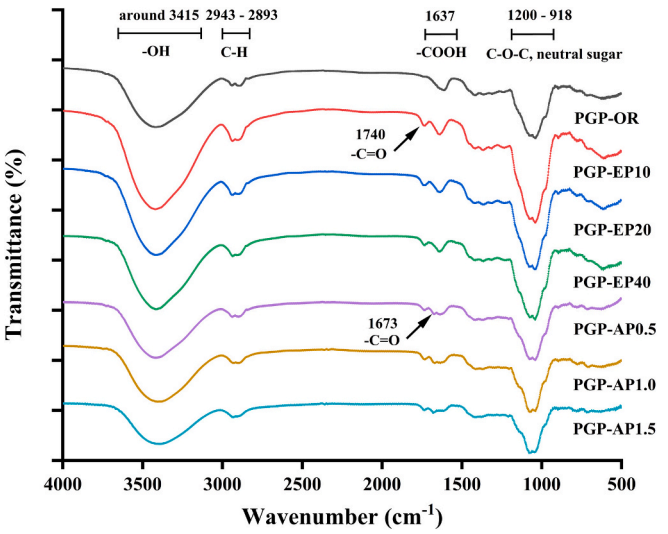

Fig. 1. Fourier transform infrared (FTIR) spectra of PGP-OR, PGP-EPs and PGP-APs. PGP-OR: original peach gum polysaccharide extracted by hot water; PGP-EP10, PGP-EP20, and PGP-EP40: the samples hydrolyzed from PGP-OR by 10, 20 and 40 μL of α-L-arabinofuranosidase treatment, respectively; PGP-AP0.5, PGP-AP1.0, and PGP-AP1.5: the samples hydrolyzed from PGP-OR by 0.5, 1.0 and 1.5 h of trifluoroacetic acid treatment, respectively;

3.5. FTIR spectroscopy of PGP samples

All PGP samples were subjected to FTIR scanning to investigate the effects of AFASE and TFA degradation on their chemical groups. The resulting spectra showed similarities, as illustrated in Fig. 1A. The prominent peak at approximately 3415 cm^{-1} was attributed to the stretching vibration of -OH groups. Bands observed at 2943 cm^{-1} and 2893 cm^{-1} were linked to C—H vibrations. Additionally, an absorption peak at 1637 cm^{-1} corresponded to the stretching vibration of carboxyl groups (-COOH). A broad band ranging from 1200 to 918 cm^{-1} could be observed in all samples, with peaks around 1147–1139 cm^{-1} associated with C-O-C glycosidic bonds, 1078–1075 cm^{-1} corresponding to β-galactan, and 1037–1032 cm^{-1} indicating arabinans (Wei, Zhang, He, et al., 2019). Similarly to PGP-OR, both PGP-EPs and PGP-APs displayed strong absorption at 1073 cm^{-1} and 1040 cm^{-1}, indicating the presence of neutral sugars such as Ara, Xyl, and Gal (Baum et al., 2016).

In addition to the similar peaks previously mentioned, the spectra of PGP-OR, PGP-EPs, and PGP-APs displayed two distinct absorption peaks. First, compared to PGP-OR, PGP-EPs, and PGP-APs exhibited a strong absorption at 1740 cm^{-1}, attributed to the carbonyl group found in the acidic sugar (Tang et al., 2020). This might be because after enzymatic and acidic treatment, the structure of PGP was more extended, exposing the carbonyl group of GlcA in the side chain. Second, in contrast to PGP-OR and PGP-EPs, the PGP-APs spectra displayed a distinct absorption peak at 1673 cm^{-1}, which might correspond to the vibration of the carbonyl group in Gal (Moustafa et al., 2021). According to the methylation results, it was observed that TFA treatment cleaved the side chains directly at their junctions with the main chain and even degraded the main chain itself. This degradation exposed terminal Gal residues, which resulted in the stretching vibration of the carbonyl group. The findings from FTIR analyses further confirmed the differences in degradation sites of PGP side chains by AFASE and TFA.

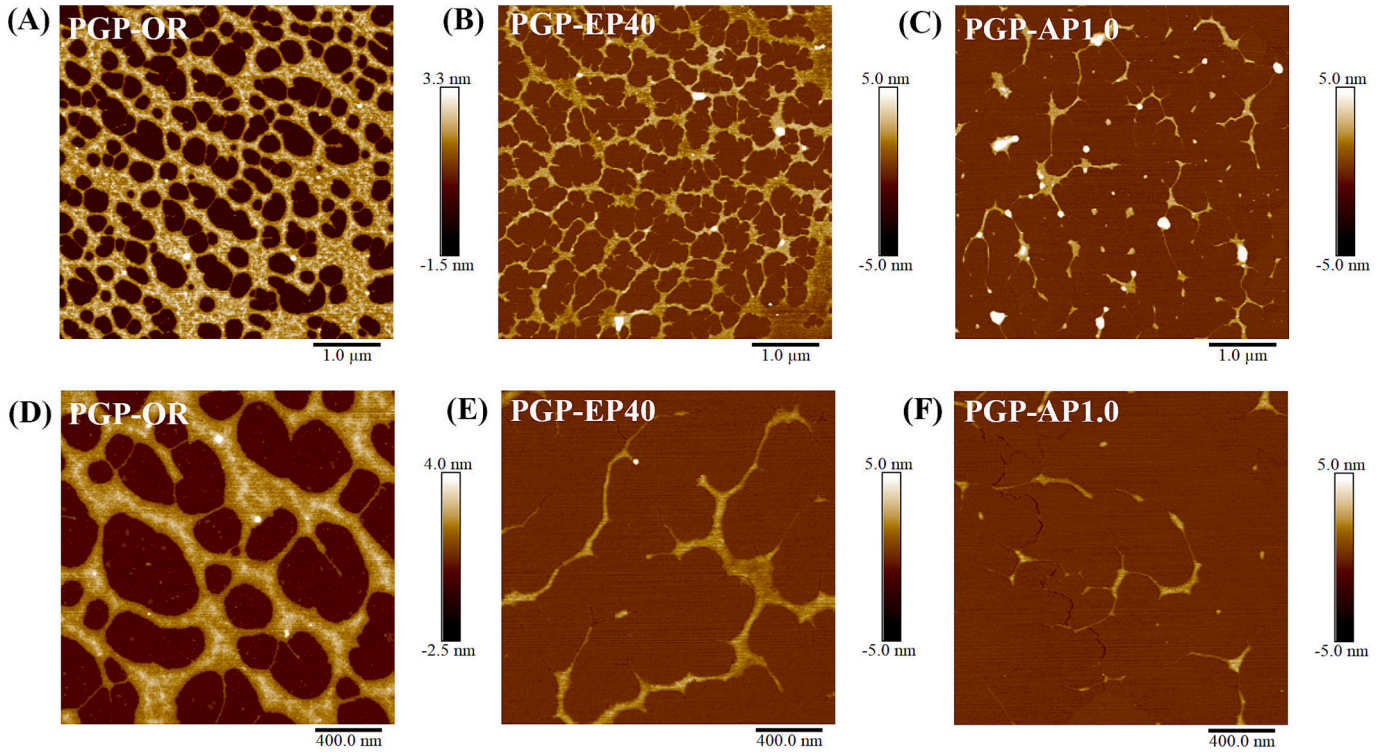

Fig. 2. Atomic force microscopy (AFM) images of PGP-OR (A) (D), PGP-EP40 (B) (E) and PGP-AP1.0 (C) (F) at 5 × 5 μm^2 and 2 × 2 μm^2 respectively. PGP-OR: original peach gum polysaccharide extracted by hot water; PGP-EP40: the sample hydrolyzed from PGP-OR by 40 μL of α-L-arabinofuranosidase treatment; PGP-AP1.0: the sample hydrolyzed from PGP-OR by 1.0 h of trifluoroacetic acid treatment;

3.6. AFM analysis of PGP-OR, PGP-EP40, and PGP-AP1.0

AFM images clearly depict the conformational changes of PGP after partial debranching. Based on the BR values, PGP-OR, PGP-EP40, and PGP-AP1.0 were selected to analyze their morphological characteristics. As shown in Fig. 2. the molecular chains in PGP-OR were cross-linked with each other in a high density, resulting in a strong network structure. These features could be ascribed to the presence of abundant side chains and relatively larger conformational parameters, such as [η], R_h, and R_g, which facilitated the cross-linking of PGP molecules (Chen, Zhou, et al., 2024). Particularly, the molecular chains of PGP-OR were intertwined together through the interaction between the abundant short Ara side chains, which formed a wide chain structure observed in Fig. 2A and D. After partial removal of the short Ara side chains by enzymatic debranching, the observable wide chain structure decreased, as well as the reduction of cross-linking density (Fig. 2B and E). However, clear network structures could be still observed, which was formed by the interaction between the long side chains that remained after enzymatic debranching. With the BR value further decreased, the network structure nearly disappeared between PGP-AP1.0 molecules (Fig. 2C and F). The above observations indicated that the Ara side chains play an important role in the cross-linking among PGP molecules. The relatively small conformational parameters including [η], R_h, and R_g, combined with the reduced side chains and disrupted backbone was unfavorable to network formation of PGP-EP40 and PGP-AP1.0 molecules. In summary, the AFM morphology results suggested that the debranching of side chains obviously weakened the intermolecular cross-linkings of PGP molecules.

3.7. Swelling volumes of PGP samples

Swelling reflects the interaction between polymer chains and water, which is influenced by the chain length, BR, M_w, and conformation (Biswal et al., 2024). The swelling volumes for all samples were measured after 30 min immersion in water. The results are presented in Fig. 3. Among all samples, PGP-OR exhibited the largest swelling volume of 0.43 cm^3. After AFASE debranching, the swelling volumes decreased to 0.19 cm^3, 0.19 cm^3, and 0.17 cm^3, respectively. After acidic debranching, the swelling volume of PGP-AP0.5 decreased to 0.18 cm^3. These results indicated that the swelling ability of PGP-OR decreased along with reductions in BR and MW. Although the main chains of PGP-AP1.0 and PGP-AP1.5 were damaged, their swelling volumes also

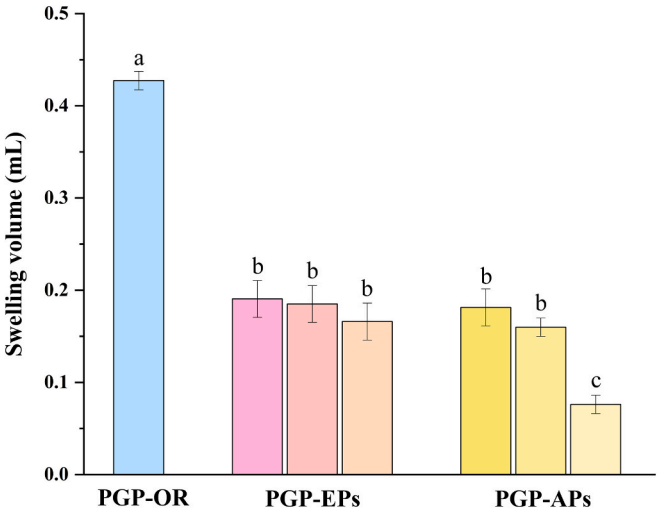

Fig. 3. Swelling volume of PGP-OR, PGP-EPs and PGP-APs. PGP-OR: original peach gum polysaccharide extracted by hot water; PGP-EPs: the samples hydrolyzed from PGP-OR by 10, 20 and 40 μL of α-L-arabinofuranosidase treatment, respectively; PGP-APs: the samples hydrolyzed from PGP-OR by 0.5, 1.0 and 1.5 h of trifluoroacetic acid treatment, respectively;

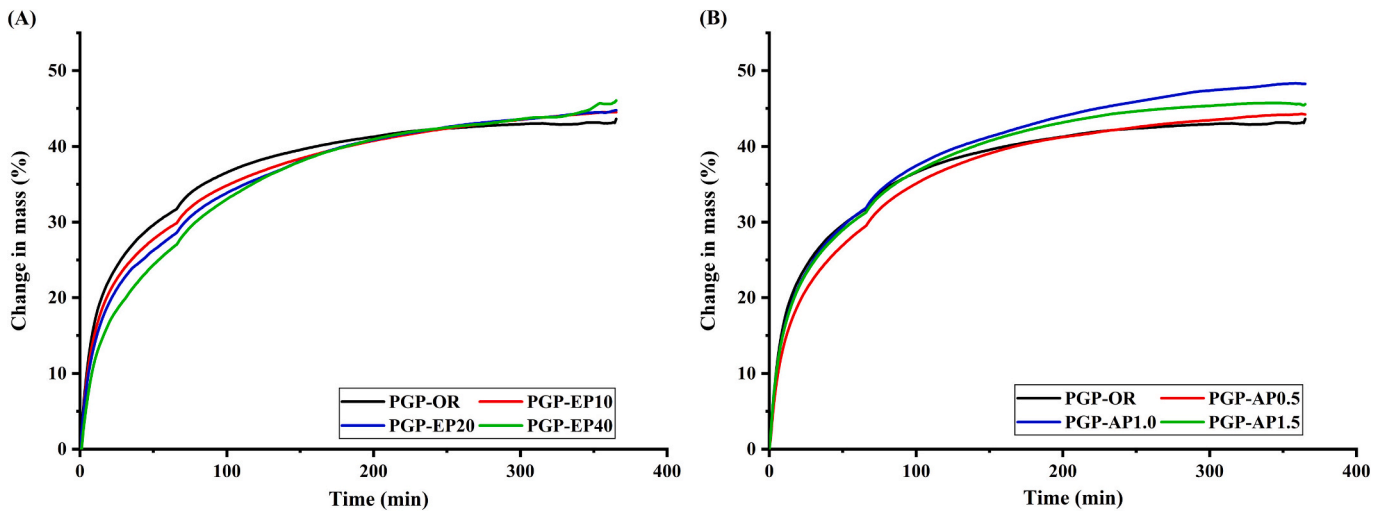

Fig. 4. Water sorption isotherms of PGP-OR, PGP-EPs and PGP-APs. PGP-OR: original peach gum polysaccharide extracted by hot water; PGP-EP10, PGP-EP20, and PGP-EP40: the samples hydrolyzed from PGP-OR by 10, 20 and 40 μL of α-L-arabinofuranosidase treatment, respectively; PGP-AP0.5, PGP-AP1.0, and PGP-AP1.5: the samples hydrolyzed from PGP-OR by 0.5, 1.0 and 1.5 h of trifluoroacetic acid treatment, respectively;

decreased to 0.16 and 0.08 cm^3, respectively. Günter et al. (2019) reported that higher MW and linearity facilitate the swelling of pectin. In the case of PGP, it suggested that the side chains also influenced its swelling ability. PGP-OR was characterized by extended molecular chains and complex cross-linked network structure. It exposed more hydrophilic groups on the Ara side chains to water, which increased interactions through hydrogen bonds with water, contributing to the swelling ability. Consequently, when PGP was immersed in water, it

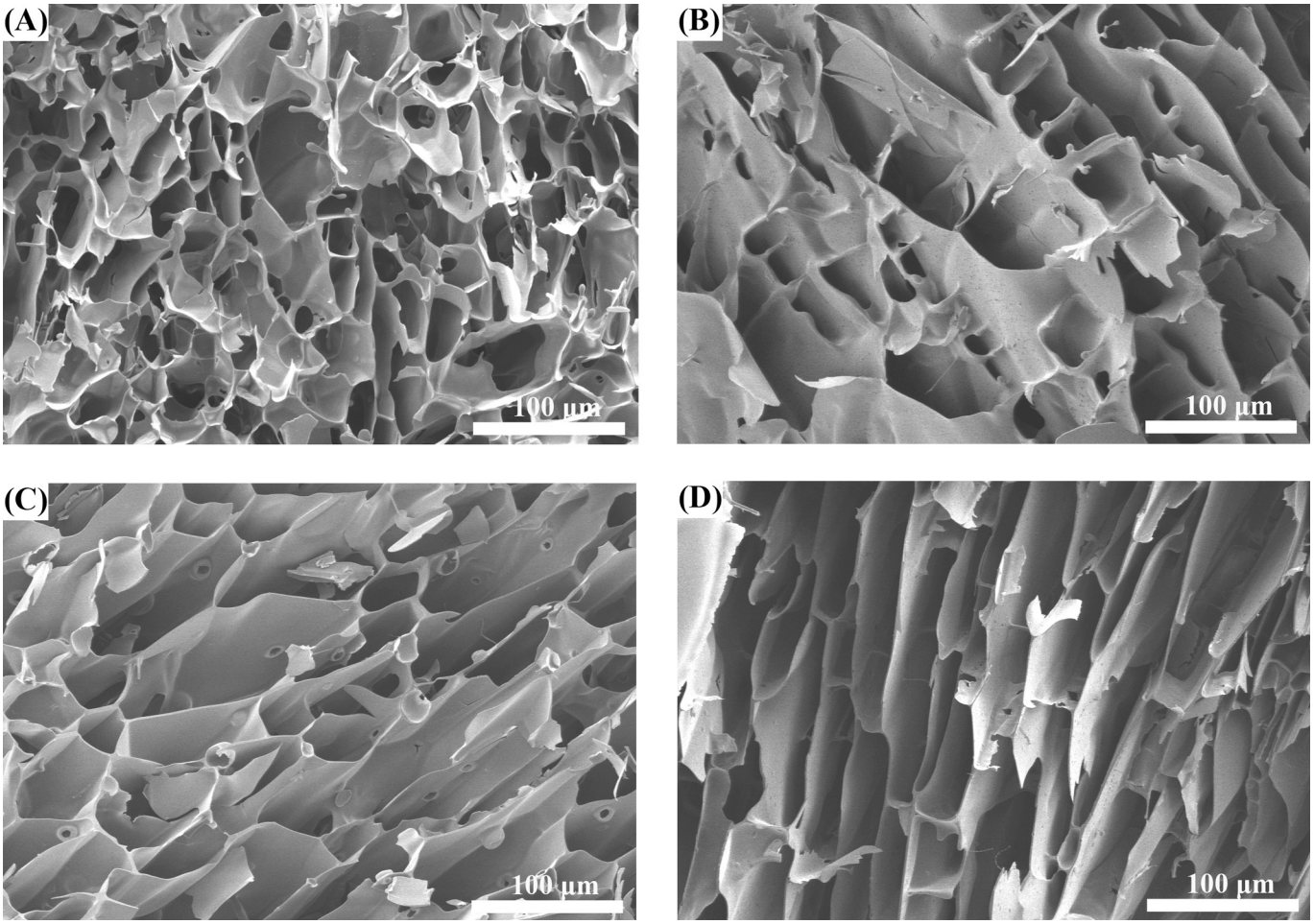

Fig. 5. Scanning electron microscope images (SEM) of PGP-OR (A), PGP-EP10 (B), PGP-AP0.5 (C), and PGP-AP1.0 (D). PGP-OR: original peach gum polysaccharide extracted by hot water; PGP-EP10: the sample hydrolyzed from PGP-OR by 10 μL of α-L-arabinofuranosidase treatment; PGP-AP0.5 and PGP-AP1.0: the sample hydrolyzed from PGP-OR by 0.5 h and 1.0 h of trifluoroacetic acid treatment, respectively;

readily captured water molecules within its complex cross-linking structure and start swelling. However, after debranching, the level of cross-linking between PGP molecules was significantly decreased. This decline weakened the interactions between the polymer network and water, resulting in a decrease in swelling volume. The partial breakage of the main chain in PGP-AP1.0 and PGP-AP1.5 further disrupted the cross-linking structure, resulting in a lower swelling volume than other debranched samples.

3.8. Water vapour sorption properties of PGP samples

In contrast to swelling volume, the water vapour sorption experiment measured the mass change after PGP sample absorbing water, which is influenced by the chemical composition, conformation and hydrophilicity/hydrophobicity ratio of the polymer (Agarwal et al., 2019; Biswal et al., 2021). The water adsorption curves for all samples were measured at relative humidity (RH) ranging from 0 % to 90 % (Fig. 4). The mass of adsorbed water steadily increased over time for each sample. From 0 to 100 min, the rate of water absorption for PGP-OR, PGP-EPs, and PGP-APs increased rapidly. After 100 min, the growth rate of mass for all samples began to slow. The PGP-EPs and PGP-APs showed greater water absorption than PGP-OR until reaching an equilibrium state. The results indicated that the water adsorption capacity of PGP-OR remained effective after debranching. Intermolecular hydrogen bonding among polysaccharide chains was recognized as a significant factor influencing water adsorption (Chen et al., 2003). The Gal units in the main chain of PGP-OR exhibited a high degree of hydrophilicity, enabling it to form hydrogen bonds with water molecules. Furthermore, debranching might expose additional hydrophilic groups, enhancing the water-binding capacity, particularly in PGP-AP1.0 and PGP-AP1.5 with disrupted main chain. The results suggested that side chains of PGP-OR did not significantly affect its water adsorption ability. Similarly, Chen et al. (2017) reported that the water absorption of *Tremella* polysaccharides increased after degradation.

3.9. SEM of PGP-OR, PGP-EP10, PGP-AP0.5, and PGP-AP1.0

It was interesting that the impacts of debranching on swelling volume and water adsorption of PGP were not completely consistent. Although swelling and water absorption both reflected the interactions between PGP sample and water, the water absorption mainly depended on the binding water ability of molecular chains, while the swelling volume mainly depended on the resilience of network structure cross-linked by PGP (Sievers et al., 2020). The network structure of PGP-OR, PGP-EP10, PGP-AP0.5, and PGP-AP1.0 samples was observed by SEM at their water adsorption equilibrium state. As shown in Fig. 5, all samples exhibited an interlinked porous network structure. The pores were irregular in shape, with most of them round or flat. The pore size of the PGP-OR was smaller and the density was higher compared with debranched samples, which indicated that PGP-OR possessed a more compact network structure. It meant that there was more space for PGP-OR networks to extend after absorbing water (Yang et al., 2025). Additionally, the dense network structure of polymer easily absorbs water molecules and did not easily lose them, further contributing to a large swelling volume (Xie et al., 2025; Zhong et al., 2016). After debranching, it was clear that the pore size was larger and the cross-linking density was lower. The loose network structure of debranched samples indicated limited expansion space after water absorption, since excessive swelling may cause the network structure to collapse (He et al., 2021). However, the large pore size meant more room for capture water molecules, resulting in a higher mass increase at the water adsorption equilibrium state, which was the reason of stronger water adsorption ability of the debranched PGP samples.

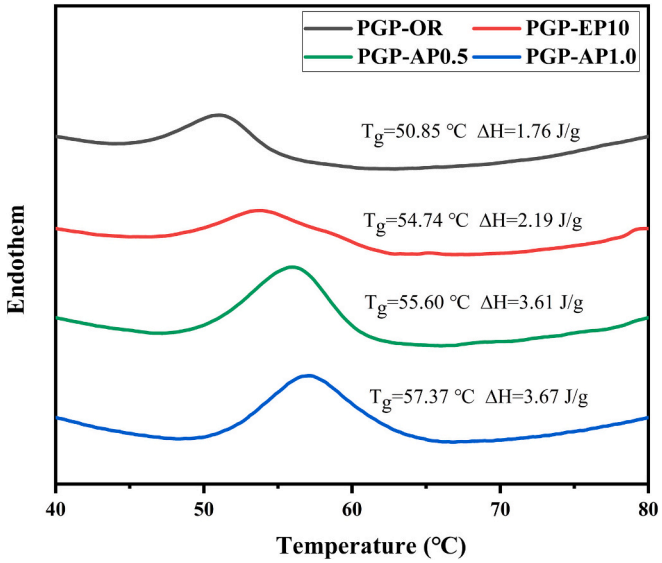

Fig. 6. Differential scanning calorimetry (DSC) curves of PGP-OR, PGP-EP10, PGP-AP0.5, and PGP-AP1.0. PGP-OR: original peach gum polysaccharide extracted by hot water; PGP-EP10: the sample hydrolyzed from PGP-OR by 10 μL of α-L-arabinofuranosidase treatment; PGP-AP0.5 and PGP-AP1.0: the sample hydrolyzed from PGP-OR by 0.5 h and 1.0 h of trifluoroacetic acid treatment, respectively;

3.10. Thermal stability analysis of PGP-OR, PGP-EP10, PGP-AP0.5, and PGP-AP1.0

The thermal stability is a critical parameter reflecting the resistant of a polymer to environmental changes. The DSC curves of PGP-OR, PGP-EP10, PGP-AP0.5, and PGP-AP1.0 are illustrated in Fig. 6. PGP-OR exhibited the lowest T_g and ΔH among all samples, with values of 50.85 °C and 1.76 J/g, respectively. After debranching, both T_g and ΔH gradually increased, followed by PGP-EP10 (54.74 °C, 2.19 J/g), PGP-AP0.5 (55.60 °C, 3.61 J/g), and PGP-AP1.0 (57.37 °C, 3.67 J/g). These results indicated that PGP-OR was more unstable and sensitive to environmental influences, requiring less energy to change from the glassy state to the rubbery state. Debranching promoted thermal stability of PGP to some extent. This might be because PGP-OR molecules with longer chains were exposed to a hot environment during heating, making them more susceptible to heat transformation and resulting in low thermal stability. This was also suggested by its microstructure. PGP-OR showed small pore size and high density, resulting in a large specific surface area, which induced a greater sensitive to thermal transformation. The side chains of debranched samples occupied smaller space, resulted in reducing the mobility contribution of the side chains to the glass transition process, thereby obtaining a higher T_g value (Enomoto-Rogers et al., 2015). Similar results were reported that the T_g of glucan branched derivatives decreased with the increasing length of the side chains (Fukata et al., 2020). Shibata et al. (2001) reported that the T_g of pullulan polysaccharide also decreased with an increasing number of groups in the side chains. Thermal stability of PGP-OR was in consistent with the presentation of DVS curves. At the initial stage, PGP-OR exhibited stronger water absorption, indicating that it was more sensitive to water in the environment. In summary, the thermal stability of debranched PGP samples were improved to some extent.

4. Conclusions

In this study, the side chains of hot water extracted PGP-OR were partially degradation using AFASE (10, 20, and 40 μL) and TFA (hydrolysis times of 0.5, 1.0, and 1.5 h) to obtain PGP-EPs and PGP-APs with different branching level. Enzymatic treatment and short time

acidic treatment (0.5 h) mainly degraded the side chains of PGP-OR, while long time acid treatment (1.0 and 1.5 h) destroyed part of the backbone in addition to the side chains. Compared to enzymatic debranching, acidic debranching was more effectiveness but less homogeneously. The debranched PGP samples retained the arabinogalactan structures, possessing smaller MW, less extended molecular chains, and less cross-linking between PGP molecules. Debranching did not reduce the water adsorption ability of PGP but decreasing the swelling volume from 0.43 cm^3 to 0.19–0.17 cm^3 for PGP-EPs and 0.18–0.18 cm^3 for PGP-APs. It was related to the network structure of PGP changing from a compact and architecture to a loose one after debranching, resulting in a better thermal stability and a less susceptibility to environment. This work provided novel knowledge for understanding "structure-property" relations of the Ara side chains to the swelling properties of PGP.

CRediT authorship contribution statement

Jingyao Li: Writing – original draft, Visualization, Validation, Investigation, Formal analysis, Data curation. **Mo Zhou:** Writing – review & editing, Project administration, Conceptualization. **Jinfeng Bi:** Supervision, Resources. **Aurore Richel:** Supervision.

Declaration of competing interest

The authors declare that they have no known competing financial interests or personal relationships that could have appeared to influence the work reported in this paper.

Acknowledgment

The research was supported by China Agriculture Research System (CARS-30-5-02), Shandong Provincial Natural Science Foundation (ZR2024MC081), and Central Public-interest Scientific Institution Basal Research Fund (S2023JBKY-11).

Data availability

Data will be made available on request.

References

Agarwal, D., MacNaughtan, W., Ibbett, R., & Foster, T. J. (2019). Effect of moisture content on thermal and water absorption properties of microfibrillar cellulose with polymeric additives. *Carbohydrate Polymers, 211*, 91–99. https://doi.org/10.1016/j.carbpol.2019.02.004

Baum, A., Dominiak, M., Vidal-Melgosa, S., Willats, W. G. T., Søndergaard, K. M., Hansen, P. W., … Mikkelsen, J. D. (2016). Prediction of pectin yield and quality by FTIR and carbohydrate microarray analysis. *Food and Bioprocess Technology, 10*(1), 143–154. https://doi.org/10.1007/s11947-016-1802-2

Biswal, A. K., Chakraborty, S., Saha, J., Panda, P. K., Pradhan, S. K., Behera, P. K., & Misra, P. K. (2024). Process optimization, fabrication, and characterization of a starch-based biodegradable film derived from an underutilized crop. *ACS Food Science & Technology, 4*(8), 1844–1863. https://doi.org/10.1021/acsfoodscitech.4c00149

Biswal, A. K., Lenka, C., Panda, P. K., Yang, J. M., & Misra, P. K. (2021). Investigation of the functional and thermal properties of Mahua deoiled cake flour and its protein isolate for prospective food applications. *Lwt, 137*. https://doi.org/10.1016/j.lwt.2020.110459

Bouaziz, F., Koubaa, M., Ellouz Ghorbel, R., & Ellouz Chaabouni, S. (2016). Recent advances in Rosaceae gum exudates: From synthesis to food and non-food applications. *International Journal of Biological Macromolecules, 86*, 535–545. https://doi.org/10.1016/j.ijbiomac.2016.01.081

Bouklas, N., & Huang, R. (2012). Swelling kinetics of polymer gels: Comparison of linear and nonlinear theories. *Soft Matter, 8*(31). https://doi.org/10.1039/c2sm25467k

Chen, J. X., Bi, J. F., Li, J. Y., & Zhou, M. (2024). Understanding the two-stage degradation process of peach gum polysaccharide within ultrasonic field. *Food Chemistry, 451*. https://doi.org/10.1016/j.foodchem.2024.139397

Chen, J. X., Zhou, M., Liu, M., & Bi, J. F. (2022). Physicochemical, rheological properties and in vitro hypoglycemic activities of polysaccharide fractions from peach gum. *Carbohydrate Polymers, 296*. https://doi.org/10.1016/j.carbpol.2022.119954

Chen, J. X., Zhou, M., Xin, G., & Bi, J. F. (2024). The impact of ultrasonic-assisted extraction on the in vitro hypoglycemic activity of peach gum polysaccharide in relation to its conformational conversion. *Journal of the Science of Food and Agriculture, 104*(11), 6947–6956. https://doi.org/10.1002/jsfa.13527

Chen, L. Y., Du, Y. M., & Zeng, X. Q. (2003). Relationships between the molecular structure and moisture-absorption and moisture-retention abilities of carboxymethyl chitosan. *Carbohydrate Research, 338*(4), 333–340. https://doi.org/10.1016/s0008-6215(02)00462-7

Chen, T. L., Xu, P., Zong, S. A., Wang, Y. F., Su, N. N., & Ye, M. (2017). Purification, structural features, antioxidant and moisture-preserving activities of an exopolysaccharide from Lachnum YM262. *Bioorganic & Medicinal Chemistry Letters, 27*(5), 1225–1232. https://doi.org/10.1016/j.bmcl.2017.01.063

Enomoto-Rogers, Y., Iio, N., Takemura, A., & Iwata, T. (2015). Synthesis and characterization of pullulan alkyl esters. *European Polymer Journal, 66*, 470–477. https://doi.org/10.1016/j.eurpolymj.2015.03.007

Fishman, M. L., Chau, H. K., Qi, P. X., Hotchkiss, A. T., Garcia, R. A., & Cooke, P. H. (2015). Characterization of the global structure of low methoxyl pectin in solution. *Food Hydrocolloids, 46*, 153–159. https://doi.org/10.1016/j.foodhyd.2014.12.021

Fukata, Y., Kimura, S., & Iwata, T. (2020). Synthesis of α-1,3-glucan branched ester derivatives with excellent thermal stability and thermoplasticity. *Polymer Degradation and Stability, 177*. https://doi.org/10.1016/j.polymdegradstab.2020.109130

Günter, E. A., Popeyko, O. V., & Istomina, E. I. (2019). Encapsulated drug system based on the gels obtained from callus cultures modified pectins. *Journal of Biotechnology, 289*, 7–14. https://doi.org/10.1016/j.jbiotec.2018.11.005

He, L. L., Su, S., Zhao, Y., & Long, J. (2023). Intrinsic relationship between viscosity, viscosity index, and molecular structure of isoalkanes. *Journal of Molecular Modeling, 29*(4). https://doi.org/10.1007/s00894-023-05494-8

He, Y. X., Li, Y., Sun, Y. D., Zhao, S. J., Feng, M., Xu, G. M., … Gu, Z. W. (2021). A double-network polysaccharide-based composite hydrogel for skin wound healing. *Carbohydrate Polymers, 261*. https://doi.org/10.1016/j.carbpol.2021.117870

Liu, M., Liu, X., Bi, J. F., Lyu, J., Wu, X. Y., Zhou, M., & Liu, J. N. (2023). Comparative study on physicochemical properties of thirteen peach gums from different varieties. *Scientia Horticulturae, 310*. https://doi.org/10.1016/j.scienta.2022.111722

Mahammad, S., Comfort, D. A., Kelly, R. M., & Khan, S. A. (2007). Rheological properties of guar galactomannan solutions during hydrolysis with Galactomannanase and α-galactosidase enzyme mixtures. *Biomacromolecules, 8*(3), 949–956. https://doi.org/10.1021/bm0608232

Méndez, D. A., Martínez-Abad, A., Martínez-Sanz, M., López-Rubio, A., & Fabra, M. J. (2023). Tailoring structural, rheological and gelling properties of watermelon rind pectin by enzymatic treatments. *Food Hydrocolloids, 135*. https://doi.org/10.1016/j.foodhyd.2022.108119

Moustafa, M., Abu-Saied, M. A., Taha, T. H., Elnouby, M., El Desouky, E. A., Alamri, S., … Al-Emam, A. (2021). Preparation and characterization of super-absorbing gel formulated from κ-carrageenan–potato peel starch blended polymers. *Polymers, 13*(24). https://doi.org/10.3390/polym13244308

Ngouémazong, D. E., Kabuye, G., Fraeye, I., Cardinaels, R., Van Loey, A., Moldenaers, P., & Hendrickx, M. (2012). Effect of debranching on the rheological properties of Ca2+−pectin gels. *Food Hydrocolloids, 26*(1), 44–53. https://doi.org/10.1016/j.foodhyd.2011.04.009

Peng, Q., Liu, H., Lei, H. J., & Wang, X. Q. (2016). Relationship between structure and immunological activity of an arabinogalactan from Lycium ruthenicum. *Food Chemistry, 194*, 595–600. https://doi.org/10.1016/j.foodchem.2015.08.087

Shibata, M., Asahina, M., Teramoto, N., & Yosomiya, R. (2001). Chemical modification of pullulan by isocyanate compounds. *Polymer, 42*(1), 59–64. https://doi.org/10.1016/s0032-3861(00)00321-9

Sievers, J., Sperlich, K., Stahnke, T., Kreiner, C., Eickner, T., Martin, H., … Stachs, O. (2020). Determination of hydrogel swelling factors by two established and a novel non-contact continuous method. *Journal Of Applied Polymer Science, 138*(18). https://doi.org/10.1002/app.50326

Simas, F. F., Gorin, P. A. J., Wagner, R., Sassaki, G. L., Bonkerner, A., & Iacomini, M. (2008). Comparison of structure of gum exudate polysaccharides from the trunk and fruit of the peach tree (Prunus persica). *Carbohydrate Polymers, 71*(2), 218–228. https://doi.org/10.1016/j.carbpol.2007.05.032

Sousa, A. G., Nielsen, H. L., Armagan, I., Larsen, J., & Sørensen, S. O. (2015). The impact of rhamnogalacturonan-I side chain monosaccharides on the rheological properties of citrus pectin. *Food Hydrocolloids, 47*, 130–139. https://doi.org/10.1016/j.foodhyd.2015.01.013

Tang, S., Wang, T., Huang, C. X., Lai, C. H., Fan, Y. M., & Yong, Q. (2020). Arabinogalactans from *Larix principis-rupprechtii*: An investigation into the structure-function contribution of side-chain structures. *Carbohydrate Polymers, 227*. https://doi.org/10.1016/j.carbpol.2019.115354

Wei, C. Y., Zhang, Y., He, L., Cheng, J. W., Li, J. H., Tao, W. Y., … Chen, S. G. (2019). Structural characterization and anti-proliferative activities of partially degraded polysaccharides from peach gum. *Carbohydrate Polymers, 203*, 193–202. https://doi.org/10.1016/j.carbpol.2018.09.029

Wei, C. Y., Zhang, Y., Zhang, H., Li, J. H., Tao, W. Y., Linhardt, R. J., … Ye, X. Q. (2019). Physicochemical properties and conformations of water-soluble peach gums via different preparation methods. *Food Hydrocolloids, 95*, 571–579. https://doi.org/10.1016/j.foodhyd.2018.03.049

Xie, X. L., Peng, M., Li, W., Ma, L., Qin, Z. Z., Su, T. M., … Ji, H. B. (2025). Preparation of rapidly absorbing bagasse cellulose-based composite superabsorbent material with semi-interpenetrating networks and its water absorption mechanism. *International Journal of Biological Macromolecules, 321*. https://doi.org/10.1016/j.ijbiomac.2025.146125

Yang, L. Q., & Zhang, L. M. (2009). Chemical structural and chain conformational characterization of some bioactive polysaccharides isolated from natural sources.

Carbohydrate Polymers, 76(3), 349–361. https://doi.org/10.1016/j.carbpol.2008.12.015

Yang, X. Q., Tan, Z. F., Zhao, W. P., Zheng, Y. F., Ling, S. Q., Guo, X. M., & Dong, X. P. (2025). Molecular interactions and gel network modulation in ionic polysaccharide-gelatin hydrogels for improved texture of skipjack tuna products. *Food Chemistry, 482*. https://doi.org/10.1016/j.foodchem.2025.144002

Yao, X. C., Cao, Y., & Wu, S. J. (2013). Antioxidant activity and antibacterial activity of peach gum derived oligosaccharides. *International Journal of Biological Macromolecules, 62*, 1–3. https://doi.org/10.1016/j.ijbiomac.2013.08.022

Yu, L., Yakubov, G. E., Zeng, W., Xing, X. H., Stenson, J., Bulone, V., & Stokes, J. R. (2017). Multi-layer mucilage of *Plantago ovata* seeds: Rheological differences arise from variations in arabinoxylan side chains. *Carbohydrate Polymers, 165*, 132–141. https://doi.org/10.1016/j.carbpol.2017.02.038

Zeng, S. H., Long, J. W., Sun, J. H., Wang, G., & Zhou, L. (2022). A review on peach gum polysaccharide: Hydrolysis, structure, properties and applications. *Carbohydrate Polymers, 279*. https://doi.org/10.1016/j.carbpol.2021.119015

Zhang, H., Li, C. C., Ding, J., Lai, P. F. H., Xia, Y. J., & Ai, L. Z. (2020). Structural features and emulsifying stability of a highly branched arabinogalactan from immature peach (*Prunus persica*) exudates. *Food Hydrocolloids, 104*. https://doi.org/10.1016/j.foodhyd.2020.105721

Zhong, M., Liu, Y. T., Liu, X. Y., Shi, F. K., Zhang, L. Q., Zhu, M. F., & Xie, X. M. (2016). Dually cross-linked single network poly(acrylic acid) hydrogels with superior mechanical properties and water absorbency. *Soft Matter, 12*(24), 5420–5428. https://doi.org/10.1039/c6sm00242k

Zhu, K., Yu, D., Chen, X. Y., & Song, G. L. (2019). Preparation, characterization and controlled-release property of Fe3+ cross-linked hydrogels based on peach gum polysaccharide. *Food Hydrocolloids, 87*, 260–269. https://doi.org/10.1016/j.foodhyd.2018.08.019